Received: 16 October 2019 | Revised: 23 May 2020 | Accepted: 26 May 2020

DOI: 10.1002/sia.6843

ECASIA SPECIAL ISSUE PAPER

SURFACE and INTERFACE ANALYSIS WILEY

Hard and soft X-ray photoelectron spectroscopy for selective probing of surface and bulk chemical compositions in a perovskite-type Ni catalyst

Olga Sambalova[1,2] | Emanuel Billeter[1,2] | Jennifer Mann[3] | Takuya Miyayama[4] | Dariusz Burnat[5] | Andre Heel[5] | Davide Bleiner[1,2] | Andreas Borgschulte[1,2]

[1]Laboratory of Advanced Analytical Technologies, Empa Materials Science and Technology, Dübendorf, Switzerland

[2]Department of Chemistry, University of Zürich, Zürich, Switzerland

[3]Analytical Laboratory, Physical Electronics, Chanhassen, Minnesota, USA

[4]Analytical Laboratory, Ulvac-PHI Laboratory, Chigasaki, Japan

[5]Institute of Materials and Process Engineering (IMPE), Zurich University of Applied Sciences (ZHAW), Winterthur, Switzerland

Correspondence
Olga Sambalova, Empa Materials Science and Technology, Ueberlandstrasse 129, CH 8600 Dübendorf, Switzerland.
Email: olga.sambalova@empa.ch

Funding information
Swiss National Science Foundation, Grant/Award Number: 172662 and 182987

Combined chemical analyses of both the surface and bulk of industrial catalysts is a significant challenge, because all microanalysis methods reveal either the surface or the bulk properties but not both. We demonstrate the combined use of hard and soft X-ray photoelectron spectroscopy (XPS) as a powerful, practical, and nondestructive tool to quantitatively analyze the chemical composition at the surfaces (~1 nm) and subsurfaces/bulk (~10 nm) for catalysts. The surface-bulk differentiation is achieved via an exchangeable anode system, where the Al (Kα, 1486.6 eV) and Cr (Kα, 5414.7 eV) for the XPS and hard X-ray photoelectron spectroscopy (HAXPES) analyses, respectively, are interchanged without affecting the X-ray beam position on the sample. As an archetypical catalyst, we study the perovskite-type material $La_{0.30}Sr_{0.55}Ti_{0.95}Ni_{0.05}O_{3-\delta}$ (LSTNO), which has differing chemical compositions at the surface and subsurface after reduction and oxidation reactions. We look at the relative changes in surface composition, which minimizes the error stemming from the differing relative sensitivity factors in the oxidized and reduced states. The HAXPES-XPS analysis indirectly confirms the well-known exsolution and formation of Ni nanoparticles on the surface upon reduction though following changes of Ni concentration at the surface. However, the XPS-HAXPES analysis demonstrates an increase in not only the Ni but also the Sr, which corroborates the reorganization within the perovskite lattice upon reduction. The XPS-measured intensities decrease for all the accessible peaks (La 3d, Sr 3d, lattice O 1s, and Ti 2p), which is attributed to the photon diffusion by the surface Ni nanoparticles.

KEYWORDS
ESCA, LSTNO, perovskite, surface/subsurface analysis, XPS-HAXPES

1 | INTRODUCTION

Soft X-ray photoelectron spectroscopy (XPS) is a widely used X-rays in–electrons out microanalysis technique that is suitable for nondestructive, quantitative, and surface sensitive elemental analyses, including the determination of oxidation states. The surface sensitivity is a consequence of the finite photoelectron escape depth, which is on the order of a few monolayers when probing with soft X-rays.[1] The probing depth is defined by the photoelectron inelastic mean free path, λ, which is a function of the incident electron kinetic energy, E (Seah and Dench[2]):

$$\lambda = \frac{143}{E^2} + 0.054\sqrt{E}.$$

Therefore, it is possible to adjust the probe depth by increasing the energy of the photoelectrons to hard X-rays (Figure 1, left).[2]

Such a hard X-ray photoemission spectroscopy (HAXPES) is commonly enabled with tunable synchrotron X-ray sources bound to large-scale facilities; however, laboratory-scale systems are relatively rare.[3,4] Notably, although already at the early stages of XPS development, higher energy laboratory-based X-ray sources were tested, including Mo (Kα = 17 479 eV),[5] Ag (Lα = 2984.3 eV),[6] Rh (Lα = 2696.8 eV),[6] and Zr (Lα = 2042.4 eV)[7]; most commercially available XPS systems comprise of Al source (Kα = 1486.6 eV). The reason lies in the exponential decay of photoionization cross section of the elements with increasing excitation energy (Figure 1, right). However, commercially available laboratory-based systems for HAXPES do exist.

Notably, recently, a combined standard Al (Kα = 1486.6 eV) and high-energy Ga (Kα = 9251.7 eV) XPS systems became available.[8] In this letter, we highlight the possibility of a laboratory XPS system that comprised a combination of soft X-rays from Al (Kα = 1486.6 eV) and hard X-rays from Cr (Kα = 5414.7 eV) anodes for probing surface and subsurface changes of catalysts. We aim at bridging the surface and the bulk analyses in catalysis by studying the technical catalysts, that is, powder samples, and comparing the results to previous works.[9,10] In particular, probing the surface and subsurface compositions of catalysts during reduction and oxidation cycles is the key to determine the structure-performance relationships in (electro)catalysis, which include the surface state and catalysis of oxides (MoO_3,[11] ZnO,[12] etc.) as well as the strong metal support interactions in metal-oxide systems.[13] To demonstrate this method for studying catalysts, we selected a well-characterized material, $La_{0.30}Sr_{0.55}Ti_{0.95}Ni_{0.05}O_{3-\delta}$ (LSTNO), which has a perovskite-type ABX_3 crystal structure, where the A-site cations are La^{3+} and Sr^{2+}, the B-site cations are Ti^{4+} and Ni^{2+}, and the X is atomic oxygen. The understoichiometry leads to improved electrical performance relative to the stoichiometric counterpart and facilitates formation of Sr vacancies (A-site deficiency of 0.85).[14] Perovskite-derived Ni catalysts offer the benefit of regeneration after catalyst poisoning through reversible Ni segregation from the oxide host.[9] The Ni ions exsolute from the crystal structure and aggregate into 5- to 10-nm particles at the surface during reduction (Figure S1).[9] Under oxidizing conditions, the nanoparticles are "re-incorporated" into the crystal host matrix, only to reappear on the surface as regenerated, catalytically active Ni nanoparticles upon further cycling. Here, reduction was performed in 10 vol.% H_2/Ar at 800°C for 15 h, and oxidation was conducted in 20 vol.% O_2/N_2 at 800°C for 2 h (for detailed experimental parameters, refer to the Supporting Information). The reversible effects of the redox cycling for the LSTNO have already been evidenced using X-ray diffraction, X-ray absorption, and electron microscopy.[9] However, no information about the lattice structural or compositional changes upon redox cycling has been provided, although it is known that the formation of vacancies or layers induces strain on the neighboring lattice parameters.[15] Controversially, studies of similar materials have reported surface enrichment of lanthanum[16] or strontium.[17–19] The sample is a non-homogeneous powder and as such is not suitable for angular resolved XPS, which is often used for surface depth profiling of homogeneous films. In contrast, the XPS-HAXPES combination is appropriate for studying non-homogeneous and/or powder surfaces and subsurfaces, which is particularly relevant for LSTNO and many other catalysts. Thus, the technique fills the current research gap by providing information about the surface and subsurface changes in the elemental compositions of all LSTNO lattice atoms between the oxidized and reduced states.

2 | METHODOLOGY

The key to differentiate the surface/bulk composition lies in the exchangeable Al/Cr anode X-ray source. The optics (such as the

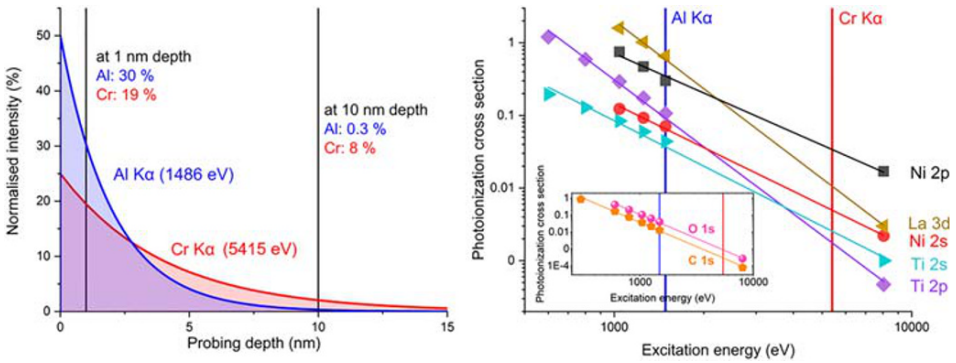

FIGURE 1 Left panel: Probing depth as a function of XPS (blue) and HAXPES (red) signal intensity. In XPS, most of the signal intensity originates from the top layers. Elements at 1 nm depth contribute about 30% towards the signal intensity, while those at 10 nm remain invisible (0.3% contribution). In HAXPES, the curve is more spread out, with about 19% and 8% signal contribution originating from a layer at 1 and 10 nm, respectively. Right panel: Photoionization cross section of Ni 2s, Ni 2p, Ti 2s, Ti 2p, and La 3d as a function of incident photon energy. The inset demonstrates the lighter elements: C 1s and O 1s photoionization cross-section functions. All of the functions follow an exponential decay, resulting in orders of magnitude difference in photoionization cross section between XPS (Al Kα) and HAXPES (Cr Kα)

ellipsoidal quartz crystal monochromator position) are adjusted to maintain the positioning of the X-ray beam regardless of whether soft (Al anode) or hard (Cr anode) X-rays are used for the analysis. The high-sensitivity, high-voltage electron analyzer equipped with a high-transmission input lens[20] allows for sufficient detection of the HAXPES and XPS photoelectrons even though there are orders of magnitude differences in the photoionization cross sections between the two techniques (Figure 1, right).[21]

3 | RESULTS AND DISCUSSION

Overall, quantification of the Ni dopant is challenging, as it is present in very low concentrations. However, the advantage of HAXPES lies in probing many more electronic states than the XPS (Figure 2), which in some cases is crucial, such as when there are overlapping lines in the XPS range. In the case of LSTNO, all Ni lines (Ni 2p and Ni 2s) overlap with the other signals in the XPS (La $3d_{3/2}$ and O KLL, respectively; Figure S2). This general difficulty of assessing Ni concentrations in the presence of lanthanum renders stoichiometric quantification of LSTNO in XPS not possible. In the HAXPES, the Auger lines shift (see O KLL and Ti LMM) and the Ni 2s states are no longer obstructed. This shift occurs because the kinetic energy of the Auger electrons does not depend on the excitation energy of the incoming X-rays, while the kinetic energy of the core photoelectrons does. Therefore, through HAXPES, all the elements present in the complex system under investigation are accessible, which is not true in case of XPS due to obstruction of all Ni signals (both minor Ni 2s and stronger Ni 2p with O KLL and La $3d_{3/2}$, respectively; Figure S2).

In technical samples, surface contamination is persistent and fast-developing. Differentiation of unwanted contaminants from the pristine surface is straightforward when using the XPS-HAXPES combination, as demonstrated in the differences between the XPS and HAXPES in the C 1s (Figure 2 inset) peaks. The strong C 1s XPS peak from adventitious carbon at 283.3 eV is diminished in the HAXPES relative to the signals from the bulk Sr $3p_{1/2}$.

The exsolution of Ni from perovskites is a process that depends on both the bulk and surface defects.[22]

$$La^{3+}_{0.30}Sr^{2+}_{0.55}Ti^{4+}_{0.95}Ni^{2+}_{0.05}O^{2-}_{3-\delta_o} \rightleftharpoons La^{l_r}_{n_{La,r}}Sr^{s_r}_{n_{Sr,r}}Ti^{t_r}_{n_{Ti,r}}O^{o_r}_{3-\delta_r} + 0.05Ni^0, \quad (1)$$

where the index r refers to reduced state. The perovskite stoichiometry n_i is governed by the number/size of crystal sites ("ABO_3") and the principle of electroneutrality in the system.[23] The XPS-HAXPES combination provides information on the elemental concentrations and the chemical states via the intensities and chemical shifts of the corresponding peaks, respectively. The absolute determination of the chemical shifts is bias-prone due to changes in the work function upon redox cycling. Here, the binding energy correction was performed with respect to the O 1s (bulk oxygen) centered at 528.50 eV as its energy is expected to be stable upon the cycling. The fitting was accomplished using the numerical convolution of a Lorentzian with a Gaussian lineshapes LA (3,3,0) after the Shirley background subtraction was performed (see Supporting Information for more information). One element in particular draws special attention as evidenced by the HAXPES. That is, the Ti 2p remains unchanged, but the Ti 1s counts decrease after the reduction. This is counterintuitive, as both these electronic states are expected to behave in the same manner, reflecting the changes in the elemental concentration. Considering the mean free paths of 3.80 nm and 1.13 nm for the Ti 2p and Ti 1s, respectively, it is evident that the spectral behavior of the latter is XPS-like, even when measured with the HAXPES (refer to Supporting Information for details). As such, it is much more dependent on surface perturbations. In fact, the spectral intensities for all LSTNO peaks measured using XPS decrease in the reduced state (Figure S3), which mirrors the transition from a pristine surface to a nanoparticle-covered one. Consequently, quantification of the LSTNO through XPS is not possible, as the different behavior of Ti 2p and Ti 1s indicates that the sample morphology significantly affects the relative sensitivity factors required for precise quantification[24]:

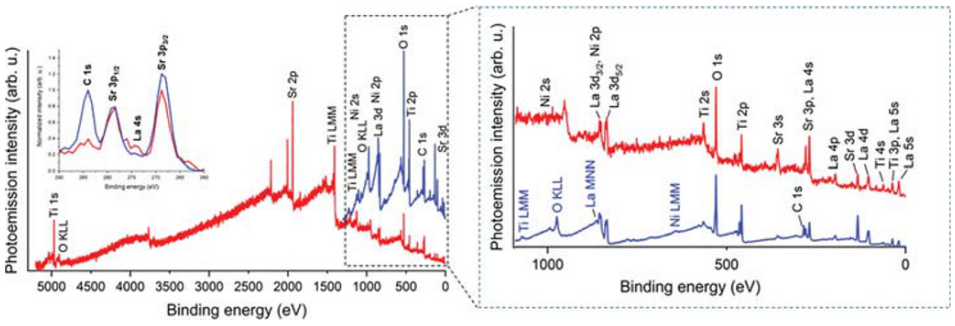

FIGURE 2 The HAXPES (red) and XPS (blue) survey spectra of the oxidized powder $La_{0.30}Sr_{0.55}Ti_{0.95}Ni_{0.05}O_{3-\delta}$. The HAXPES allows probing more electronic states. The inset shows the region of C 1s, which originates from adsorbed carbon species. Here, the intensity is normalized to the Sr $3p_{1/2}$ peak. Left panel shows the enlarged 1100 to 0 eV binding energy region for easier comparison

$$\frac{n_i}{n_j} = \frac{S_i}{S_j}\frac{I_i}{I_j}, \tag{2}$$

where n is number of atoms of element i or j, S is the relative sensitivity factor, and I is the signal intensity. The relative sensitivity factor includes contributions from the X-ray flux (f), photoelectron cross section for the atomic orbitals of interest (σ), angular efficiency factor based on the X-ray source to electron analyzer angle (θ), efficiency in the photoelectric process for the formation of photoelectrons at the nominal photoelectron energy (y), mean free path of the photoelectrons in the sample (λ), sample area (A), and detection efficiency (T)[24] and is given by

$$S = f\sigma\theta y\lambda AT. \tag{3}$$

The effective mean free path and sample area are subject to change in catalysis samples, such as from a modified surface roughness, surface area, and particle diameter. Therefore, the sensitivity factors in oxidized and reduced conditions cannot be assumed to be the same. To minimize this uncertainty, we restrict the evaluation to the relative changes, rather than absolute:

$$\frac{\frac{n_{i,r}}{n_{i,o}}}{\frac{n_{j,r}}{n_{j,o}}} = \frac{\frac{S_{i,r}}{S_{i,o}}\frac{I_{i,r}}{I_{i,o}}}{\frac{S_{j,r}}{S_{j,o}}\frac{I_{j,r}}{I_{j,o}}}. \tag{4}$$

Thus, the data treatment outlined in Equation 4 allows the cancelation all parameters defining S (Equation 3), except for the effective mean free path and sample area. Although absolute quantification via this method is not possible, the relative changes allow for a meaningful interpretation.

Contrary to previous studies on similar systems,[18,25] we observed no changes in the chemical state of Ti between oxidized and reduced samples (Figure 3). From the binding energy of the Ti 2p at 457.2 eV, we derived that the chemical state is mainly of the form Ti^{4+}. A small contribution from Ti^{3+} may be present (shoulder at 455.4 eV) but remains unchanged between the oxidized and reduced states. The transformation of Ti^{4+} into Ti^{3+} is a direct consequence of oxygen removal from the crystal lattice.[14] However, in the presence of Ni^{2+}, a decrease in the B-site valence will occur preferentially when transitioning from Ni^{2+} to Ni^{0}. Due to the higher Ti—O bond strengths relative to Ni-O,[26] the O—Ti—O lattice structure remains relatively stable, while segregated Ni

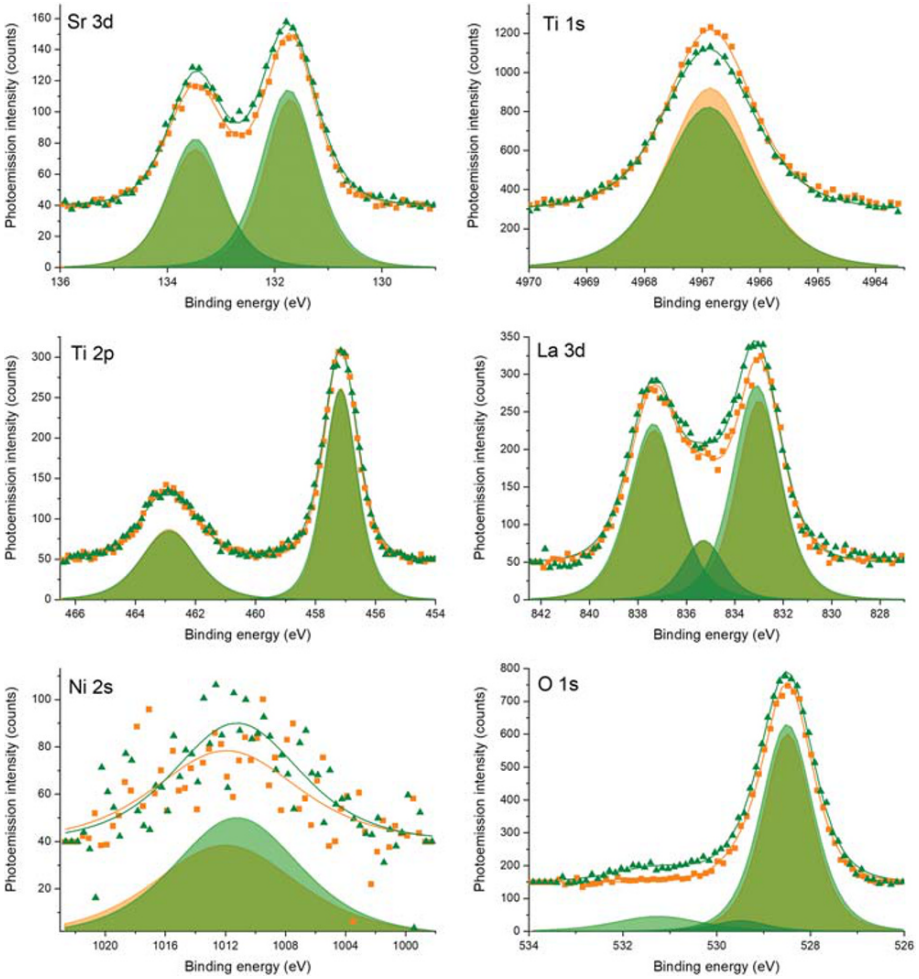

FIGURE 3 High-resolution HAXPES spectra of the LSTNO in oxidized (orange) and reduced (green) states. The measured HAXPES data are presented as orange squares and green triangles, with the total fitting shown as an orange or green solid lines, respectively. Both the measurement point and the overall fitting lines are offset for clarity. The fittings of individual peaks and doublets originating from spin-orbit splitting are presented as filled curves, likewise in orange and green for oxidized and reduced states, respectively. For all elements, reduced state peaks (green) are of the same (e.g., Ti 2p) or higher (e.g., Sr 3d) intensity, with the notable exception of Ti 1s. For detailed information regarding the extended peak assignment, peak areas, peak area ratios, and residuals, see Table S1

nanoparticle formation is observed. It can also be noted that the fraction of superficial oxygen removed from the lattice is low relative to the large number of Ti-occupied sites, which could also explain no observable Ti^{4+} reduction. Moreover, the presence of A-site vacancies counteract the reduction of Ti^{4+} in understoichiometric LST.[14]

Significant shifts of the binding energy are observed for the Ni 2s (+0.8 eV) and La 3d (−0.1 eV) peaks towards higher and lower binding energies, respectively (Figure 3 and Table S3). The first observation is in perfect agreement with the well-known formation of metallic Ni^0 from Ni^{2+}.[9] The second observation is counterintuitive. In Equation 1, we considered the oxidation state of La to be trivalent with no further oxidation possible. However, the chemical state is also dependent on the chemical environment. Lanthanum cations are smaller and have a higher charge than strontium cations, indicating they prefer to stay "buried" in the bulk, rather than becoming exposed at the surface.[27] The decreased electron density of La after reduction, which is reflected by a shift towards a higher binding energy, could signify an increased proximity to oxygen atoms, in particular, the O 1s lateral structure peak[25,28] centered at 529.5 eV. This additional O 1s state has been reported for several metal oxides and has been assigned to the lower coordinated oxygen atoms, that is, those with lower electron densities than the O^{2-} states of the crystalline network.[25]

The chemical shifts for all the elements are nearly the same between the XPS and HAXPES (Table S3). However, the shifts for La are more prominent in the HAXPES at −0.11 eV compared with −0.04 eV for the XPS. This signifies larger changes in the subsurface environment for this element.

Both the XPS and HAXPES indirectly confirm the well-established exsolution of Ni particles and indicate an enrichment in not only the Ni, but also in Sr, especially at the surface (Figure 4). Interestingly, the Sr content increased significantly relative to the O at the surface and decreased only mildly at the subsurface. This Sr enrichment is in contrast to previously reported La surface enrichments of LSTNs with higher La^{3+} content, $La_{052}Sr_{0.28}Ti_{0.94}Ni_{0.06}O_3$.[16] It is noted that the material properties depend on several factors, such as the elemental doping levels, synthesis route, surface treatment, and material

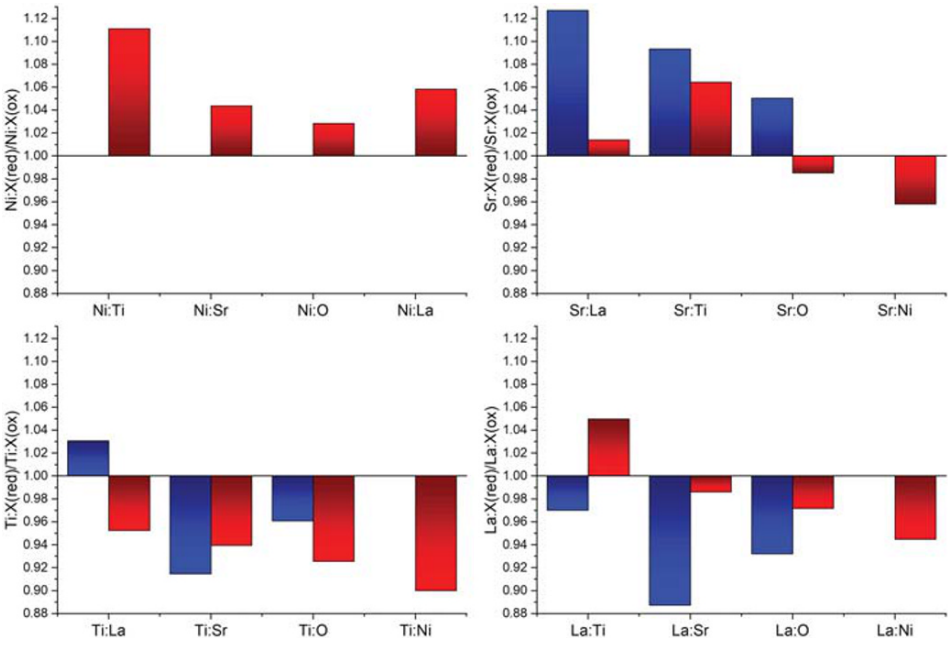

FIGURE 4 Surface elemental enrichment and depletion from the HAXPES (red) and XPS (blue) measurements. The changes in the presence of each of the elements are presented relative to the change in the other four elements of the LSTNO. For detailed calculations, see Tables S1 and S2

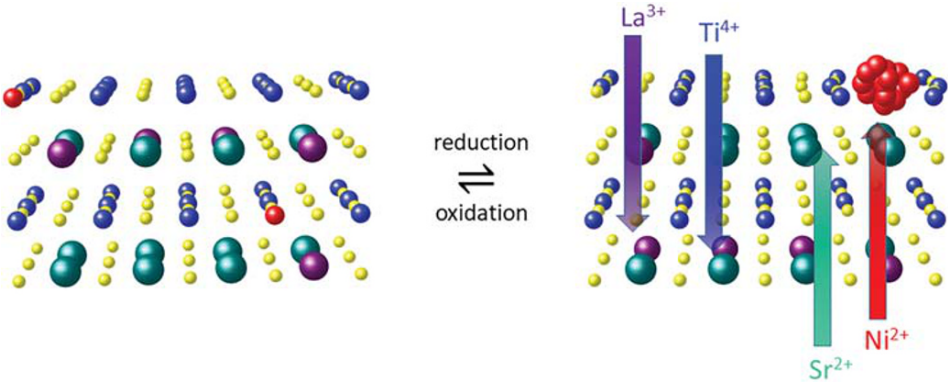

FIGURE 5 The LSTNO ideal cubic crystal structure (space group $Pm\bar{3}m$), with La^{3+} (purple), Sr^{2+} (green), Ti^{2+} (blue), Ni^{2+} (red), and O^{2-} (yellow). Oxygen anions are represented disproportionally small relative to their actual size for clarity of the scheme. Upon LSTNO reduction, the Sr^{2+} and Ni^{2+} diffuse in parallel to the surface, where the latter aggregates to form nanoparticles. At the same time, the surface is depleted of La^{3+} and Ti^{4+}

handling. As either Sr^{2+} (Bucher et al.[17] and Huber et al.[18]) or La^{3+} (Neagu et al.[16]) enrichment have been observed, even for seemingly similar systems, no general conclusions applicable to all LSTN-type catalysts can be reached, and each specific system has to be studied individually. At the same time, both Ti and La decreased at the surface and subsurface (Figure 4). However, through the combination of the XPS and HAXPES results, it is clear that La^{3+} migrated into the subsurface more than the Ti^{4+}, leaving a La-depleted surface (Figure 5).

4 | CONCLUSIONS

In summary, we demonstrated the power of a combined XPS-HAXPES analysis to selectively determine changes in the elemental concentration at the surface and subsurface due to redox reactions. The technique provides results consistent with prior characterizations (Ni surface enrichment), while at the same time allowing the selective study of less pronounced and more analytically challenging changes in the ion concentrations at the surface and in the bulk. Simultaneously, Ni and Sr are enriched, while La and Ti are depleted at the surface. Moreover, we discuss the relative sensitivity factors of the same element in the reduced and oxidized states, which cannot be assumed to be equal, as seen from the different behavior of Ti 1s and Ti 2p. Therefore, it is crucial to analyze the changes in the elements relative to each other to indicate when the differences in the relative sensitivity factors cancel out.

ACKNOWLEDGEMENTS

This work was partly supported by the UZH-UFSP program LightChEC. Financial support from the Swiss National Science Foundation (grant numbers 172662 and 182987) is greatly acknowledged.

ORCID

Olga Sambalova https://orcid.org/0000-0002-9012-4028

REFERENCES

1. Powell CJ, Jablonski A. Surface sensitivity of X-ray photoelectron spectroscopy. *Nucl Instrum Methods Phys Res, Sect A*. 2009;601(1–2):54-65. https://doi.org/10.1016/j.nima.2008.12.103
2. Seah MP, Dench WA. Quantitative electron spectroscopy. *Surf Interface Anal*. 1979;1(1):2-11.
3. Zier M, Oswald S, Reiche R, Wetzig K. Non-destructive depth profile analysis using synchrotron radiation excited XPS. *Microchim Acta*. 2006;156(1–2):99-101. https://doi.org/10.1007/s00604-006-0615-9
4. Flodstrom SA, Bachrach RZ, Bauer RS, McMenamin JC, Hagström SBM. Investigation of plasmon sidebands by synchrotron radiation tuning of electron escape depths. *J Vac Sci Technol A*. 2002;14(1):303-306. https://doi.org/10.1116/1.569147
5. Nordling C, Sokolowski E, Siegbahn K. Precision method for obtaining absolute values of atomic binding energies. *Phys Ther Rev*. 1957;105(5):1676-1677. https://doi.org/10.1103/PhysRev.105.1676
6. Keski-Ranhkonen O. Energies and chemical shifts of the sulphur 1s level and the $KL_2L_2(^1D_2)$ auger line in HZS, SO_2 and SF_6. *J Electron Spectros Relat Phenom*. 1976;9(4):371-380.
7. West RH, Castle JE. The correlation of the auger parameter with refractive index: an XPS study of silicates using Zr Lα radiation. *Surf Interface Anal*. 1982;4(2):68-75. https://doi.org/10.1002/sia.740040208
8. Regoutz A, Mascheck M, Wiell T, et al. A novel laboratory-based hard X-ray photoelectron spectroscopy system. *Rev Sci Instrum*. 2018;89(7):073105. https://doi.org/10.1063/1.5039829
9. Steiger P, Burnat D, Madi H, et al. Sulfur poisoning recovery on a solid oxide fuel cell anode material through reversible segregation of nickel. *Chem Mater*. 2019;31(3):748-758. https://doi.org/10.1021/acs.chemmater.8b03669
10. Burnat D, Kontic R, Holzer L, Steiger P, Ferri D, Heel A. Smart material concept: reversible microstructural self-regeneration for catalytic applications. *J Mater Chem A*. 2016;4(30):11939-11948. https://doi.org/10.1039/c6ta03417a
11. Borgschulte A, Sambalova O, Delmelle R, Jenatsch S, Hany R, Nüesch F. Hydrogen reduction of molybdenum oxide at room temperature. *Sci Rep*. 2017;7(1):40761. https://doi.org/10.1038/srep40761
12. Behrens M, Studt F, Kasatkin I, et al. The active site of methanol synthesis over cu/ZnO/Al_2O_3 industrial catalysts. *Science*. 2012;336(6083):893-897.
13. Tauster SJ. Strong metal-support interactions. *Acc Chem Res*. 1987;20(11):389-394. https://doi.org/10.1021/ar00143a001
14. Burnat D, Heel A, Holzer L, Kata D, Lis J, Graule T. Synthesis and performance of A-site deficient lanthanum-doped strontium titanate by nanoparticle based spray pyrolysis. *J Power Sources*. 2012;201:26-36. https://doi.org/10.1016/j.jpowsour.2011.10.088
15. Ohnishi T, Shibuya K, Yamamoto T, Lippmaa M. Defects and transport in complex oxide thin films. *J Appl Phys*. 2008;103(10):103703. https://doi.org/10.1063/1.2921972
16. Neagu D, Oh TS, Miller DN, et al. Nano-socketed nickel particles with enhanced coking resistance grown in situ by redox exsolution. *Nat Commun*. 2015;6(1):8120. https://doi.org/10.1038/ncomms9120
17. Bucher E, Sitte W, Klauser F, Bertel E. Impact of humid atmospheres on oxygen exchange properties, surface-near elemental composition, and surface morphology of $La_{0.6}Sr_{0.4}CoO_{3-\delta}$. *Sol St Ion*. 2012;208:43-51. https://doi.org/10.1016/j.ssi.2011.12.005
18. Huber AK, Falk M, Rohnke M, et al. In situ study of activation and deactivation of LSM fuel cell cathodes—electrochemistry and surface analysis of thin-film electrodes. *J Catal*. 2012;294:79-88. https://doi.org/10.1016/j.jcat.2012.07.010
19. Opitz AK, Rameshan C, Kubicek M, et al. The chemical evolution of the $La_{0.6}Sr_{0.4}CoO_{3-\Delta}$ surface under SOFC operating conditions and its implications for electrochemical oxygen exchange activity. *Top Catal*. 2018;61(20):2129-2141. https://doi.org/10.1007/s11244-018-1068-1
20. Ulvac-Phi,(n.d.) Physical electronics. https://www.ulvac-phi.com/en/products/xps/quantes/
21. Yeh JJ, Lindau I. Atomic subshell photoionization cross sections and asymmetry parameters: $1 \leqslant Z \leqslant 103$. *At Data Nucl Data Tables*. 1985;32(1):1-155. https://doi.org/10.1016/0092-640X(85)90016-6
22. Myung JH, Neagu D, Miller DN, Irvine JTS. Switching on electrocatalytic activity in solid oxide cells. *Nature*. 2016;537(7621):528-531. https://doi.org/10.1038/nature19090
23. Pena MA, Fierro JLG. Chemical structures and performance of perovskite oxides. *Chemical Reviews*. 2017;101(7):1981-2018. https://doi.org/10.1021/cr980129f
24. Moulder JF, Stickle WF, Sobol PE, Bomben KD. In: Chastain J, ed. *Handbook of X-ray photoelectron spectroscopy*. Eden Prairie: Perkin-Elmer Corporation; 1992.
25. Dupin JC, Gonbeau D, Vinatier P, Levasseur A. Systematic XPS studies of metal oxides, hydroxides and peroxides. *Phys Chem Chem Phys*. 2000;2(6):1319-1324. https://doi.org/10.1039/a908800h

26. Luo Y. *Handbook of Bond Dissociation Energies in Organic Compounds*. 1st Ed. Boca Raton: CRC Press; 2002. https://doi.org/10.1201/9781420039863
27. Ding H, Virkar AV, Liu M, Liu F. Suppression of Sr surface segregation in $La_{1-x}Sr_xCo_{1-y}Fe_yO_{3-\delta}$: a first principles study. *Phys Chem Chem Phys*. 2013;489-496. https://doi.org/10.1039/c2cp43148c
28. van der Heide PAW. Systematic X-ray photoelectron spectroscopic study of $La_{1-x}Sr_x$-based perovskite-type oxides. *Surf Interface Anal*. 2002;33(5):414-425. https://doi.org/10.1002/sia.1227

SUPPORTING INFORMATION

Additional supporting information may be found online in the Supporting Information section at the end of this article.

How to cite this article: Sambalova O, Billeter E, Mann J, et al. Hard and soft X-ray photoelectron spectroscopy for selective probing of surface and bulk chemical compositions in a perovskite-type Ni catalyst. *Surf Interface Anal*. 2020;1–7. https://doi.org/10.1002/sia.6843